arXiv:1212.6746v1 [quant-ph] 30 Dec 2012

Deterministic quantum teleportation between distant atomic objects

H. Krauter[1], D. Salart[1], C. A. Muschik[2], J. M. Petersen[1], Heng Shen[1], T. Fernholz[3], and E. S. Polzik[1]
[1] *Niels Bohr Institute, Copenhagen University, Blegdamsvej 17, 2100 Copenhagen, Denmark.*
[2] *ICFO-Institut de Ciències Fotòniques, Mediterranean Technology Park, 08860 Castelldefels (Barcelona), Spain.*
[3] *School of Physics & Astronomy, The University of Nottingham, Nottingham, NG7 2RD, UK.*

Quantum teleportation is a key ingredient of quantum networks [1, 2] and a building block for quantum computation [3, 4]. Teleportation between distant material objects using light as the quantum information carrier has been a particularly exciting goal. Here we demonstrate a new element of the quantum teleportation landscape, the deterministic continuous variable (cv) teleportation between distant material objects. The objects are macroscopic atomic ensembles at room temperature. Entanglement required for teleportation is distributed by light propagating from one ensemble to the other. Quantum states encoded in a collective spin state of one ensemble are teleported onto another ensemble using this entanglement and homodyne measurements on light. By implementing process tomography, we demonstrate that the experimental fidelity of the quantum teleportation is higher than that achievable by any classical process. Furthermore, we demonstrate the benefits of deterministic teleportation by teleporting a dynamically changing sequence of spin states from one distant object onto another.

Quantum teleportation of discrete [5] and continuous [6] variables is the transfer of a quantum mechanical state without the transmission of a physical system carrying this state. The first experimental teleportation protocols employed light as the carrier of quantum states [7, 8]. Teleportation of atomic states over microns distances has been realized in two experiments using short range interactions between trapped ions [9]. Interspecies teleportation from light onto atoms has been achieved both deterministically for continuous variables [10] and probabilistically for discrete variables [11]. Recently, probabilistic teleportation between two ions [12] and two atomic ensembles [13] over a macroscopic distance has been demonstrated. While probabilistic teleportation, in which entanglement is distributed by photon counting [7, 14], is capable of reaching distances of many km [2, 15], the power of continuous variable (cv) teleportation is that it succeeds deterministically in every attempt [8, 10], that it is capable of teleporting complex quantum states [16], and that it can be used in universal quantum computation [4]. Here, we present an experimental demonstration of deterministic cv teleportation between distant macroscopic atomic ensembles, thus extending the powerful cv teleportation [8, 10, 16] onto atomic memory states. The protocol which succeeds in every attempt allows us to teleport dynamically changing quantum states of collective atomic spins with a bandwidth of tens of Hz.

The quantum teleportation process begins with the creation of a pair of entangled objects. In our experiment these two objects are an atomic ensemble at site B and a photonic wave packet generated by interaction of this ensemble with a driving light pulse (Fig. 1a). The wave packet travels to site A, the location of the atomic ensemble whose state is to be teleported. This step establishes a quantum link between the two locations. Following the interaction of the ensemble A and the wave packet, the cv Bell measurement is performed on the transmitted light. The result of this measurement is communicated via a classical channel to site B, where it is fed back via local operations on the second entangled object, i.e. the ensemble B, thus completing the process of teleportation.

Continuous variable teleportation is described in the language of canonical operators. For atomic ensembles, fully spin polarized along the x-axis, those are scaled dimensionless Cartesian components of the collective spin: $x = J_y/\sqrt{< J_x >}$ and $p = J_z/\sqrt{< J_x >}$ [17], where $J_{x,y,z} = \sum_i j^i_{x,y,z}$ (summed over all atoms i) is the collective angular momentum of the ensemble. Here, we employ ^{133}Cs atoms polarized into $|F = 4, m_F = 4\rangle$ electronic ground state. The usual link between the ladder operator b for collective atomic excitations [17] of the state $m_F = 3$ (Fig. 1b) and canonical variables is $b^\dagger = (x - ip)/\sqrt{2}$. Atoms are placed in a bias magnetic field collinear with J_x, so that in the lab frame the observables $x \propto J_y$ and $p \propto J_z$ rotate at Larmor frequency Ω (Fig. 1a) according to the atomic Hamiltonian $H_\text{A} = -\Omega \left(x^2 + p^2\right)/2$. Atom-light interaction is shown in Fig. 1b and involves two scattering processes $H_{int} \propto \mu a^\dagger_\text{us} b^\dagger - \nu a^\dagger_\text{ls} b + h.c.$ where $a^\dagger_\text{us/ls}$ generate photons in the upper/lower $(\omega \pm \Omega)$ sideband modes of the driving field ω. Previously, this type of interaction has been used to create entanglement between photonic modes [18], described by a_us, a_ls, and between two atomic spin ensembles [19]. This interaction contains both essential ingredients of the teleportation protocol, the creation of entanglement between the atoms and photons (first term) and a beam-splitter type operation between atoms and photons (second term). For the present experiment, the ratio of the amplitudes of the entangling and beam-splitter parts of the Hamiltonian is $\mu/\nu = 1.38$. Due to the Larmor precession, it is useful to introduce two-mode canonical variables for light (y and q), given by $y_c \cos(\Omega t) + y_s \sin(\Omega t) \propto a_\text{us} e^{-i\Omega t} + a_\text{ls} e^{i\Omega t} + h.c.$ where $y_{c,s}$ are the cosine and sine components, with similar definitions for q. Encoding quantum states of atoms in high frequency modes Ω allows for quantum noise limited performance of cv variables of macroscopic atomic ensembles. Photonic variables $y_{c,s}$ are measured via polarization homodyne detection with nearly unity quantum efficiency and are also quantum noise limited at frequency Ω.

The experiment (Fig. 1a) utilizes two room temperature gas ensembles of $N_A \approx 10^{11} - 10^{12}$ spin polarized Cesium atoms in glass cells with spin protecting coating as in [17, 18, 20] placed at a distance of 0.5m. Crucially, the macroscopic spins of the two ensembles here are parallel, whereas in our

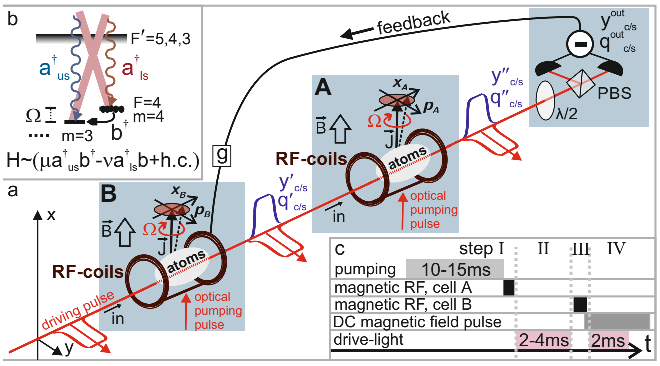

Figure 1: **Teleportation experiment**. (a) The experimental layout. A strong driving pulse propagates first through ensemble B creating the mode y', q' entangled with B and then through ensemble A whose state is to be teleported. Bell measurement on the modes y'', q'' is performed by polarization homodyning. Teleportation is completed by classical communication of these results to B. More comments in the text. (b) The level scheme and relevant transitions. Classical drive field (thick lines) and quantum fields forming the mode y, q (wavy lines) are shown, (c) The time line of the experiment. I. Preparation of the input state, II. Entanglement and Bell measurement, III. Feedback, IV. Read-out of the teleported state.

previous work [17, 19] where the goal was generation of entanglement between two ensembles they were antiparallel. The bias magnetic field of $B \approx 0.9$G corresponds to $\Omega = 322$kHz. Both ensembles are initially optically pumped into the $|F = 4, m_F = 4\rangle$ state using the combination of 852nm and 893nm circularly polarized light, thus creating a coherent spin state (CSS) : $\mathrm{Var}(J_y) \cdot \mathrm{Var}(J_z) = J_x^2/4$ with $J_x \approx 4N_A$ and $\langle J_y \rangle = 0$ and $\langle J_z \rangle = 0$, corresponding to a vacuum state with variances $\mathrm{Var}(x) = \mathrm{Var}(p) = 1/2$. The spin of the ensemble A to be teleported is then displaced with mean values $\langle x_A \rangle$ and $\langle p_A \rangle$ by a weak radio-frequency (rf) magnetic field pulse of frequency Ω corresponding to the creation of coherent superposition of electronic ground states $m_F = 3, m_F = 4$ (Fig. 1b). This input state can also be made dynamically evolving in time, as described below.

The layout and time sequence for teleportation and verification are shown in Fig. 1a,c. A y-polarized, 3ms long light pulse drives the interaction with a power of 5.6mW, blue detuned from the D_2 line $F = 4 \rightarrow 5$ transition by $\Delta = 850$MHz. The forward scattered mode, x-polarized and described by y', q' is entangled with the collective spin B and co-propagates with the drive light towards the site A. The interaction with the ensemble A leads to partial mapping of its state onto light, and is followed by the Bell measurements on the light modes y'', q'' of the upper and lower sidebands performed via polarization homodyning with the driving light acting as the local oscillator. The detailed theoretical model of the teleportation protocol is presented in the Supplementary Information (SI). Near unity teleportation fidelity can be achieved [23], if the driving fields for A and B ensembles are made time-dependent. However, even with top hat driving pulses a sufficiently high fidelity can be achieved, if an optimal temporal mode for the detected homodyne signal is chosen. The optimal readout mode is $y_{c/s,-} \propto \int_0^T \cos/\sin(\Omega t) e^{-\gamma t} y(t) dt$, where T is the pulse duration and γ is the decay rate of the atomic state. Measurements of such observables with specific temporal mode functions can easily be conducted by electronic post-processing of the photocurrent. The teleportation protocol is completed by sending the measurement results $y''_{c/s,-}$ via a classical link to the site B where spin rotations in the y, z plane conditioned on these signals are performed using phase and amplitude controlled rf magnetic field pulses at frequency Ω. The gain coefficient for this classical feedback is optimized for every class of teleported states to maximize the average fidelity. The deterministic character of the homodyne process ensures success of the teleportation in every attempt.

We performed teleportation of sets of CSS with varying $< J_{y,z} >$, corresponding to displaced vacuum or coherent states in quantum optical terms. Calibration of the input states of ensemble A and the post-teleportation read-out of the resulting state of ensemble B are done by polarization homodyning of transmitted pulses, $y^A_{c/s,-}$ and $y^B_{c/s,-}$, respectively, with the same temporal mode as for the Bell measurement. Using Eq.1 from the Methods Summary, the mean values of the input states of ensemble A are found as $< x_A > = < y^A_{c,-} > /\kappa$, $< p_A > = < y^A_{s,-} > /\kappa$ and their variances as $\mathrm{Var}(x_A) = (\mathrm{Var}(y^A_{c,-}) - c_y^2/2 - c_q^2/2 - c_N^2 m/2)/\kappa^2$, $\mathrm{Var}(p_A) = (\mathrm{Var}(y^A_{s,-}) - c_y^2/2 - c_q^2/2 - c_N^2 m/2)/\kappa^2$ with interaction coefficients $c_{y,q,N}, m$ and κ described in the Methods Summary. As in our previous work with room temperature spin ensembles, the prepared atomic input states are found to be very close to ideal CSS' with $\mathrm{Var}(x_A) = \mathrm{Var}(p_A) = (1.03 \pm 0.03) \cdot 1/2$, which confirms the validity of the read-out procedure and allows for teleportation process tomography. After each teleportation sequence, the characteristic variables $< x_B^{\mathrm{tele}} >, < p_B^{\mathrm{tele}} >, \mathrm{Var}(x_B^{\mathrm{tele}}), \mathrm{Var}(p_B^{\mathrm{tele}})$ of the spin state of the target ensemble B are found in the same way from the read-out of the verification pulse $y^B_{c/s,-}$. Based on those values the experimental fidelity is determined using a standard method of calculation of state overlap [23]. Optimization of the teleportation protocol has been performed by varying the drive pulse duration T, the measured temporal mode of light, and the gain for the classical feedback. The optimal read-out mode was always found with an exponential decay rate equal to the spin decay γ as expected from the model.

The quantum character of the teleportation is verified by comparing the fidelity of state transfer to the classical benchmark teleportation fidelity. More specifically, we perform the teleportation process tomography [10, 21] using various sets of coherent spin states of ensemble A as input states. For such Gaussian states the individual state transfer fidelity is calculated from the first two moments [23], i.e. the mean values and the variances $\sigma_x^2 = \mathrm{Var}(x_B^{\mathrm{tele}})$, $\sigma_p^2 = \mathrm{Var}(p_B^{\mathrm{tele}})$. We then evaluate the average transfer fidelity for sets of coherent states with a Gaussian distribution of displacements with mean number $\bar{n} = < b^\dagger b >$ of spin excitations [22, 23]. A rigorous classical benchmark fidelity $(1 + \bar{n})/(1 + 2\bar{n})$ for such classes of states has been derived in [22]. Demonstration of a fidelity above the classical benchmark signifies the success of quan-

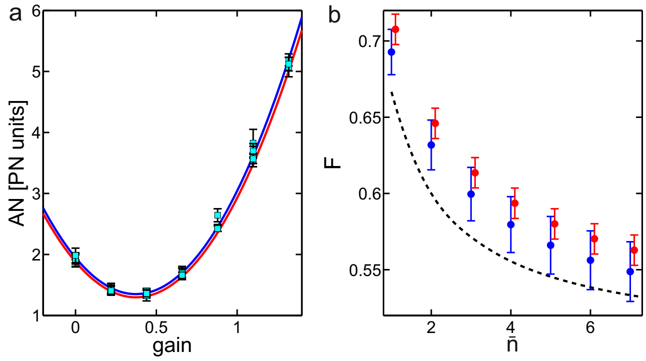

Figure 2: **Teleportation fidelity**. (a) The variances of the teleported state Var$(x^{\text{tele}}, p^{\text{tele}})$ in projection (vacuum) noise units as a function of gain. (b)Teleportation fidelity as a function of the mean photon number of the input set of states. Blue curves/points - feedback applied before the verification measurement, red curves/points - feedback applied after the verification measurement. Black dashed line represents the classical benchmark. Error bars represent one standard deviation.

tum teleportation and is equivalent to the ability of the teleportation channel to transfer entangled states. The Gaussian character of the atomic spin states has been experimentally verified, and experimental runs for different CSS input states with displacements of $0, 5, 25, 160$ in canonical units and phases $0, \pi/4, \pi/2$ in x, p space and different gains g have been performed. For every input state, 10.000-20.000 teleportations can be performed within a time slot of a few minutes with one full cycle of the protocol lasting 20ms. Fig. 2a shows the variances of the teleported states as a function of gain g for different input states. The quadratic dependence of the variances on g predicted by the model [23] fits the experimental data very well. It is clear from the figure that for a certain range of gain values, the atomic variances are reduced, which indicates entanglement of the transmitted light with the ensemble B [23]. Fig. 2b presents the experimental fidelity (blue dots), which is above the classical benchmark for $\bar{n} \leq 7$. Instead of applying the classical feedback conditioned on the Bell measurements to the spin B and then performing the verification measurement, we can choose to first perform the verification measurement on spin B and then apply the classical feedback to the results. In theory, those two procedures are equivalent, but in the experiment the resulting fidelity for the latter one is slightly higher (red dots in Fig. 2b) since the application of rf fields required in the former procedure introduces additional technical errors.

The deterministic teleportation can be used for "stroboscopic" teleportation of spin dynamics from A to B. To illustrate this specific feature, we performed repeated teleportation cycles while varying the amplitude and phase of the input state. The results are presented in Fig. 3. The left column displays the rf field which is applied to prepare a new spin state A each time, after initializing both ensembles to vacuum between teleportation runs. The central column shows the readout of the input state evolution of ensemble A and the right column shows the read-out of the teleported state evolution. The grey points represent results for individual teleportation runs.

The fidelity of the teleportation can be further improved by using time varying drive pulses [23] and increasing the optical depth of the atomic ensembles. Cv teleportation is capable of teleporting highly non-classical states as shown for teleportation of light modes [16], so it can be expected that deterministic teleportation of an atomic qubit [14] can be performed by developing the present approach. The stroboscopic teleportation of spin dynamics can also be extended towards a true continuous in time teleportation paving the way to teleportation of quantum dynamics and simulations of the interaction between two distant objects which do not interact directly [24]. From the quantum sensing perspective teleportation of spin dynamics allows for performing measurements at remote locations, spatially separated from the environment where the actual dynamics take place.

Methods Summary

The calibration of the input atomic spin state, the Bell measurement, and the detection of the state teleported onto the spin B are performed via polarization homodyning measurements of the Stokes operator $S_2 = (n_{+45} - n_{-45})/2$ given by the difference of photon numbers polarized in ±45° directions (Fig.1) [20, 25]. The measured canonical variable for light is then defined as $S_2 \approx \sqrt{\Phi}/2 \cdot y$ where Φ is the driving field photon flux, which experimentally means that all measurements are normalized to shot noise of light. The photocurrent is analyzed with a lock-in amplifier at the Larmor frequency Ω and further computer processed to obtain measurements of the temporal modes of interest $y_{c/s,-}$. All light pulses for teleportation and read-out always pass through both vapour cells (Fig. 1). For the read out of each individual ensemble the other ensemble is detuned from the atom-light interaction by briefly detuning the B field in the respective cell. For off-resonant light well below saturation used here, the linear transformation of light variables after dispersive interaction with atoms is given by [19, 25]:

$$y_{c/s,-} = \kappa \cdot p/x + c_y \cdot y^{\text{in}}_{c/s,f_y} + c_q \cdot q^{\text{in}}_{s/c,f_q} + c_N \cdot F_{p,x}. \quad (1)$$

Here, the first term is a contribution of the atomic spin variable due to Faraday rotation of light polarization, the second term is proportional to the input value of the light quadrature y of the temporal mode f_y and the third term is the contribution of the other quadrature of input light q of temporal mode f_q resulting from back action of light on atoms [23]. All input light modes are always in a coherent or vacuum state with $Var(y^{\text{in}}_{c/s,f_y}) = Var(q^{\text{in}}_{c/s,f_q}) = 1/2$. The last term in Eq. 1 describes additional noise arising from atomic decoherence with $Var(F_{p,x}) = m/2$ with $m = 1.3$ found from the atomic spin relaxation [26]. The value of the interaction constant κ is found by calibrating the Faraday rotation caused by the ensemble [19]. The constants c_y and c_q are determined by sending light with displacements of $< y^{\text{in}}_{c/s,f_y} >$ and $< q^{\text{in}}_{c/s,f_q} >$, storing it in the atomic medium, then reading it out onto an-

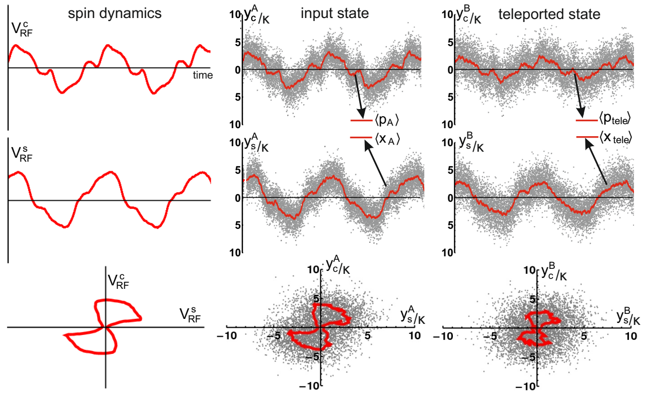

Figure 3: **Teleportation with a dynamically varied input state.** Left column - rf magnetic field applied to spin A with components $x_A \propto J_y \propto V^s_{rf}, p_A \propto J_z \propto V^c_{rf}$. The center/right columns present the read-out of the input/teleported dynamics of the atomic spins A/B in vacuum units. Every grey point is a teleportation run with the points taken at the rate of ~ 50Hz. The red lines present the running average of the grey points. The first/second row is the $p_{A,B}/x_{A,B}$ variable and the third row is a two-dimensional plot $x_{A,B}, p_{A,B}$. The optimal teleportation gain for this evolution is 0.8 which is seen as a smaller mean amplitude of the teleported evolution compared to the original.

other pulse $< y^{\text{out}}_{c/s,-} >$ and measuring the ratios. The values for c_y, c_q and c_N can also be calculated from the model [23]

based on three experimental parameters: the total transverse decay rate of the atomic spin state γ, the contribution of spin decoherence (spontaneous emission, collisions and inhomogeneity of the magnetic field) to this decay time γ_{extra} and $Z^2 = (\mu + \nu)/(\mu - \nu)$. $Z^2 = 6.3$ is calculated from Clebsch-Gordon coefficients for the atomic transitions and experimentally verified [18]. For 5.6mW read out pulses of 2ms duration and room temperature Cs vapor pressure (effective resonant optical depth of 34 for 22mm long cells) $\gamma = 99.3 \pm 0.2\text{sec}^{-1}$ and $\gamma_{\text{extra}} = 26.3 \pm 0.2\text{sec}^{-1}$ have been measured. A unitary contribution to the decay $\gamma - \gamma_{\text{extra}}$ is due to the collective coupling H_{int}, which describes the rate of entanglement generation and the beam splitter interaction [23] and depends on the optical depth of the ensemble, the optical detuning, and the intensity of the driving field. The measured values of κ, c_y, c_q agree very well with the predictions of the model [23] and are $\kappa = 0.87$, $c_y = 0.93$, $c_q = 0.50$ for our teleportation setting. The last coefficient in the readout equation can be found from the measured parameters as $c_N = c_q \cdot \sqrt{2 \cdot \gamma_{\text{extra}}/(\gamma - \gamma_{\text{extra}})}/Z = 0.17$. For the atomic state reconstruction the detection efficiencies including optical losses $\eta_B = 0.80 \pm 0.03$ and $\eta_A = 0.89 \pm 0.03$ for ensembles A/B are taken into account.

Acknowledgements

We gratefully acknowledge discussions with J. I. Cirac, K. Hammerer and D. V. Vasilyev. This work was supported by the ERC grants INTERFACE and QUAGATUA, the Danish National Science Foundation Center QUANTOP, the DARPA program QUASAR, the Alexander von Humboldt Foundation, TOQATA (FIS2008-00784) and the EU projects QESSENCE and AQUTE.

Author Contributions

H.K., D.S., J.M.P, H.S. and T.F. performed the experiment. The theoretical model has been developed by C.A.M. H.K, C.A.M., D.S. and E.S.P have written the paper. E.S.P. supervised the project.

---

[1] Briegel, H.-J., Dür, W., Cirac, J. I. & Zoller, P. Quantum Repeaters: The Role of Imperfect Local Operations in Quantum Communication. *Physical Review Letters*, **81**, 5932–5935 (1998).

[2] de Riedmatten, H. *et al.* Long Distance Quantum Teleportation in a Quantum Relay Configuration *Physical Review Letters*, **92**, 47904 (2004).

[3] Gottesman, D. & Chuang, I.L. Demonstrating the viability of universal quantum computation using teleportation and single-qubit operations *Nature*, **402**, 390–393 (1999).

[4] Gottesman, D., Kitaev, A., Preskill, J. Encoding a qubit in an oscillator. *Physical Review A*, **64**, 012310 (2001).

[5] Bennett, C. H. *et al.* Teleporting an unknown quantum state via dual classical and Einstein-Podolsky-Rosen channels *Physical Review Letters*, **70** , 1895–1899 (1993).

[6] Vaidman, L. Teleportation of quantum states *Physical Review A*, **49**, 1473–1476 (1994).

[7] Bouwmeester, D. *et al.*, A Experimental quantum teleportation *Nature*, **390**, 575–579 (1997).

[8] Furusawa, A. *et al.* Unconditional Quantum Teleportation *Science* , **282**, 706–709 (1998).

[9] Riebe, M. *et al.* Deterministic quantum teleportation of atomic qubits *Nature*, **429**, 737–739 (2004). Barret, M.D. *et al.* Deterministic quantum teleportation with atoms *Nature*, **429**, 734–737 (2004).

[10] Sherson, J. *et al.* Quantum teleportation between light and matter *Nature*, **443**, 557–560 (2006).

[11] Chen, Y.A. *et al.* Memory-built-in quantum teleportation with photonic and atomic qubits *Nature Physics*, **4**, 103–107 (2008).

[12] Olmschenk, S. *et al.* Quantum Teleportation Between Distant Matter Qubits *Science*, **323** , 486–489 (2009).

[13] Bao X-H. *et al.* Quantum teleportation between remote atomic-ensemble quantum memories *Proceedings of the National Academy of Sciences of the United States of America*, **109**, 20347–20351 (2012).

[14] Duan, L.M., Lukin, M.D., Cirac, J.I. & Zoller, P. Long-distance quantum communication with atomic ensembles and linear optics *Nature*, **414**, 413–418 (2001).

[15] Ma, X.S. *et al.* Quantum teleportation over 143 kilometres using active feed-forward *Nature*, **489** , 269–273 (2012).

[16] Lee, N. *et al.* Teleportation of Nonclassical Wave Packets of Light *Science*, **332**, 330–333 (2011).

[17] Hammerer, K., Sørensen, A.S. & Polzik, E.S. Quantum interface between light and atomic ensembles *Reviews of Modern Physics*, **82**, 1041–1093 (2010).

[18] Wasilewski, W. *et al.* Generation of two-mode squeezed and entangled light in a single temporal and spatial mode *Optics Express*, **17**, 14444–14457 (2009).

[19] Krauter, H. *et al.* Entanglement Generated by Dissipation and Steady State Entanglement of Two Macroscopic Objects *Physical Review Letters*, **107**, 080503 (2011).

[20] Sherson, J., Julsgaard, B. & Polzik, E.S. Deterministic Atom-Light Quantum Interface *Advances in Atomic, Molecular, and Optical Physics*, **54**, 81–130 (2006).

[21] Lobino, M. *et al.* Complete characterization of quantum-optical processes *Science*, **322**, 563–566 (2008).

[22] Hammerer, K., Wolf, M.M., Polzik, E.S. & Cirac, J.I. Quantum benchmark for storage and transmission of coherent states *Physical Review Letters*, **94**, 150503 (2005).

[23] More details are given in the Supplementary information.

[24] Muschik, C.A., Polzik, E.S. & Cirac J.I. Dynamical quantum teleportation and continuous effective interactions between remote systems, in preparation.

[25] Muschik, C.A. *et al.* Robust entanglement generation by reservoir engineering *Journal of Physics B: Atomic, Molecular and Optical Physics*, **45**, 124021 (2012).

[26] Vasilyev, D.V., Hammerer, K., Korolev, N. & Sørensen, A.S. Quantum Noise for Faraday Light Matter Interfaces *Journal of Physics B: Atomic, Molecular and Optical Physics* **45** 124007 (2012).

Supplemental Information

In the following, we provide additional information on the the read-out of the atomic spin state and the protocol used for teleportation. In Sec. A, we discuss the input-output relations for the interaction of a single cell with light. These equations are the basis for the read-out which is used for verification. In Sec. B, we explain the teleportation scheme, state the corresponding input-output relations for atoms and light and calculate the attainable fidelity.

A. Light-matter interaction

We are interested in reading out the spin state of an atomic ensemble, which is described in terms of bosonic operators x and p. This information is mapped to a coherent light field. The interaction of light with atoms, which are rotating in a magnetic field with a Larmor frequency Ω leads to temporally modulated light modes. More specifically, the atomic quadratures x and p are mapped to $\sin(\Omega t)$ and $\cos(\Omega t)$ modulated light modes respectively, which can be accessed individually. As explained below, we consider here specific light modes with an exponentially falling slowly varying envelope on top of the fast sine/cosine modulation. The relevant input-output relation for these read-out modes are given by

$$\begin{aligned}\begin{pmatrix} y_{\text{c},-} \\ y_{\text{s},-} \end{pmatrix} &= \kappa \begin{pmatrix} p^{\text{in}} \\ x^{\text{in}} \end{pmatrix} + c_{\text{y}} \begin{pmatrix} y^{\text{in}}_{\text{c},f_{\text{y}}} \\ y^{\text{in}}_{\text{s},f_{\text{y}}} \end{pmatrix} + c_{\text{q}} \begin{pmatrix} -q^{\text{in}}_{\text{s},f_{\text{q}}} \\ q^{\text{in}}_{\text{c},f_{\text{q}}} \end{pmatrix} \\ &+ c_{\text{N}} \begin{pmatrix} F^{\text{in}}_{p} \\ F^{\text{in}}_{x} \end{pmatrix}. \qquad \text{(S.1)}\end{aligned}$$

These equations include atomic decay. The first term on the right side is the desired atomic signal. The second and third term on the right represent contributions of the light field. The first subscript of the photonic operators refers to the fast modulation (i.e. modulation with $\sin(\Omega t)$ or $\cos(\Omega t)$), while the second subscript refers to the mode function of the slowly varying envelope (as explained below). F_x^{in} and F_p^{in} are atomic noise operators, κ, c_{y}, c_{q} and c_{N} are real coefficients and are given by Eqs. (S.5) below.

The interaction between atoms and light is governed by the Hamiltonian $H = H_{\text{A}} + H_{\text{L}} + H_{\text{int}}$, where H_{L} represents the free propagation of the light field along z and H_{A} is the free Hamiltonian of the atomic system. More specifically, $H_{\text{A}} = -\Omega\left(x^2+p^2\right)/2$, describes the Larmor precession with Larmor frequency Ω of the atoms in the magnetic field. The interaction Hamiltonian is a combination of a passive (beamsplitter-) part H_{BS}, which preserves the number of excitations in the system and an active (two mode squeezing) part H_{TMS}, which creates entanglement between atoms and light,

$$\begin{aligned} H_{\text{int}} &= \sqrt{2\gamma_{\text{s}}}\left(\mu H_{\text{BS}} - \nu H_{\text{TMS}}\right) \\ &= \sqrt{2\gamma_{\text{s}}}\left(Zpq(0) + \frac{1}{Z}xy(0)\right), \qquad \text{(S.2)} \end{aligned}$$

where $\mu = \frac{1}{2}\left(Z+\frac{1}{Z}\right)$, $\nu = \frac{1}{2}\left(Z-\frac{1}{Z}\right)$. Here, we assumed a pointlike atomic ensemble which is located at the origin $z = 0$. The light field is described in terms of spatially localized modes $y(z,t)$, $q(z,t)$ with $[y(z,t),q(z',t)] = c\delta(z-z')$ [S1, S2, S3]. We perform a variable transformation to a moving frame $\bar{y}(\xi,t) = y(ct-\xi,t)$ on the spatial argument of the light-field operators (see for example [S3, S4]). Using this description, integrated light modes can be defined by considering an integral over the individual pieces of the light pulse with temporally varying weighting functions (see Eq. (S.3) and Eq. (S.4)).

We derive the input-output relations for the light-matter interaction given by Eq. (S.2) in the limit $\Omega T \gg 1$, where T is the total interaction time. Contributions which are on the order of $(\Omega T)^{-1}$ are neglected, which is a very good approximation for the experimental parameters considered here (compare [S3, S5, S6]). We include undesired noise processes, which lead to a decay of the transverse atomic spin at a rate γ_{extra}. In the presence of noise, the optimal slowly varying envelope for the read-out is an exponentially falling mode $e^{-\gamma t}$, where $\gamma = \gamma_{\text{s}} + \gamma_{\text{extra}}$. In the experiment, the exponentially falling sine and cosine modulated light modes

$$\begin{pmatrix} y_{\text{c},-} \\ y_{\text{s},-} \end{pmatrix} = \frac{2\sqrt{\gamma}}{\sqrt{1-e^{-2\gamma T}}}\int_0^T dt e^{-\gamma t}\begin{pmatrix} \cos(\Omega t) \\ \sin(\Omega t) \end{pmatrix}\bar{y}(ct,T) \text{(S.3)}$$

are measured. The corresponding input-output relations are given by Eq. (S.1) above. The light and noise modes appearing in this equation are defined by

$$\begin{aligned}
\begin{pmatrix} y^{\text{in}}_{\text{c},f_\text{y}} \\ y^{\text{in}}_{\text{s},f_\text{y}} \end{pmatrix} &= \frac{1}{\sqrt{N_\text{y}}}\int_0^T dt\, f_\text{y}(t)\begin{pmatrix}\cos(\Omega t)\\ \sin(\Omega t)\end{pmatrix}\bar{y}(ct,0),\\
\begin{pmatrix} q^{\text{in}}_{\text{s},f_\text{q}} \\ q^{\text{in}}_{\text{c},f_\text{q}} \end{pmatrix} &= \frac{1}{\sqrt{N_\text{q}}}\int_0^T dt\, f_\text{q}(t)\begin{pmatrix}\sin(\Omega t)\\ \cos(\Omega t)\end{pmatrix}\bar{q}(ct,0),\\
\begin{pmatrix} F^{\text{in}}_{p} \\ F^{\text{in}}_{x} \end{pmatrix} &= \frac{1}{\sqrt{N_\text{N}}}\int_0^T dt\, f_\text{N}(t)\begin{pmatrix} f_p(t)\\ f_x(t)\end{pmatrix}, \qquad \text{(S.4)}
\end{aligned}$$

where $f_x(t)$ and $f_p(t)$ are atomic noise operators with $\langle f_x(t)\rangle = \langle f_p(t)\rangle = 0$ and $\langle f_x(t)f_x(t')\rangle = \langle f_p(t)f_p(t')\rangle = \frac{m}{2}\delta(t-t')$. Accordingly, $\text{var}\left(F_x^{\text{in}}\right) = \text{var}\left(F_p^{\text{in}}\right) = m/2$. For the interaction Hamiltonian, given by Eq. (S.2), one obtains $m = 1.3$ [S7, S8]. The modulating functions f_y, f_q and f_N read

$$\begin{aligned}
f_\text{y}(t) &= \frac{1}{\sqrt{1-e^{-2\gamma T}}}\left([2\sqrt{\gamma}-\frac{\gamma_\text{s}}{\sqrt{\gamma}}]e^{-\gamma t}+\frac{\gamma_\text{s}}{\sqrt{\gamma}}e^{-2\gamma T}e^{\gamma t}\right),\\
f_\text{q}(t) &= Z^2\frac{\gamma_\text{s}}{\sqrt{\gamma}}\frac{1}{\sqrt{1-e^{-2\gamma T}}}\left(e^{-\gamma t}-e^{-2\gamma T}e^{\gamma t}\right),\\
f_\text{N}(t) &= Z\frac{\sqrt{\gamma_\text{s}\gamma_\text{extra}}}{\sqrt{\gamma}}\frac{1}{\sqrt{1-e^{-2\gamma T}}}\left(e^{-\gamma t}-e^{-2\gamma T}e^{\gamma t}\right),
\end{aligned}$$

with

$$\begin{aligned}
N_\text{y} &= \frac{1}{2}\int_0^T dt f_\text{y}(t)^2,\\
N_\text{q} &= \frac{1}{2}\int_0^T dt f_\text{q}(t)^2,\\
N_\text{N} &= \int_0^T dt f_\text{N}(t)^2.
\end{aligned}$$

The coefficients appearing in Eq. (S.1) are given by

$$\begin{aligned}
\kappa &= \frac{Z\sqrt{\gamma_\text{s}}}{\sqrt{2\gamma}}\sqrt{1-e^{-2\gamma T}}, \qquad \text{(S.5)}\\
c_\text{y} &= \sqrt{N_\text{y}},\ \ c_\text{q} = \sqrt{N_\text{q}},\ \ c_\text{N} = \sqrt{N_\text{N}}.
\end{aligned}$$

It is instructive to consider the limiting case of large $Z^2 >> 1$, with $\gamma_\text{s} T Z^2 = \text{const}$. In this limit, $\mu = \nu$ and we obtain a quantum non demolition (QND) interaction with $H_\text{int} \propto pq$. In the absence of decay, the coefficients of the input-output relation Eq. (S.1) become

$$\kappa = Z\sqrt{\gamma T}, \quad c_\text{y} = 1, \quad c_\text{q} = \kappa^2/\sqrt{3}, \quad c_\text{N} = 0. \qquad \text{(S.6)}$$

In this case, the readout equations take a form extensively used previously [S3, S5]

$$\begin{pmatrix} y_{\text{c},-} \\ y_{\text{s},-} \end{pmatrix} = \begin{pmatrix} y^{\text{in}}_{\text{c},-} \\ y^{\text{in}}_{\text{s},-} \end{pmatrix} + \kappa\begin{pmatrix} p^{\text{in}} \\ x^{\text{in}} \end{pmatrix} + \frac{\kappa^2}{\sqrt{3}}\begin{pmatrix} -q^{\text{in}}_{\text{s},f_\text{q}} \\ q^{\text{in}}_{\text{c},f_\text{q}} \end{pmatrix}. \qquad \text{(S.7)}$$

B. Teleportation scheme

In this section, we discuss the teleportation scheme. In Sec. B 1, we explain the basic working principle of the protocol and provide the corresponding input-output relations. In Sec. B 2, we compute the teleportation fidelity.

1. Protocol and input-output relations

A standard teleportation scheme involving the three parties Alice, Bob and Charlie consists of the following three steps, which allow Alice to teleport a quantum state provided by Charlie to Bob. (i) Alice and Bob establish an entangled link, which is shared between the two remote parties. (ii) Alice performs a Bell measurement on her part of the entangled state shared with Bob and an unknown quantum state prepared by Charlie. (iii) Alice uses a classical channel to communicate the measurement outcome to Bob, who performs a local operation on his quantum state conditioned on Alice's result.

In the setup used here (see Fig.1a in the main text), the quantum state prepared by Charlie is stored in ensemble II. This state is teleported to ensemble I, which represents Bob, while the light field in x-polarization plays the role of Alice. Step (i) in the standard protocol outlined above corresponds to the interaction between the light field and the first atomic ensemble which results in an entangled state. The distribution of entanglement between the two remote sites is realized by means of the free propagation of the photonic state. Step (ii) corresponds to the interaction of the light field with the second ensemble and the subsequent measurement of the y-quadrature of the transmitted light by means of homodyne detection. Step (iii) is implemented in the form of a feedback operation realizing a conditional displacement on ensemble I using radio-frequency magnetic fields. In principle, it is not necessary to perform the displacement as long as the outcome of the measurement in step (ii) is known.
The measured values of $y^{\text{out}}_{\text{c},-}$ and $y^{\text{out}}_{\text{s},-}$ are fed back onto the first ensemble as explained above. Due to symmetry reasons, applying equal gain factors $g_x = g_p = g$ is optimal. This yields

$$\begin{aligned}
\begin{pmatrix} x^{\text{tele}}_{\text{I}} \\ p^{\text{tele}}_{\text{I}} \end{pmatrix} &= \bar{c}_\text{I}\begin{pmatrix} x^{\text{in}}_{\text{I}} \\ p^{\text{in}}_{\text{I}} \end{pmatrix} + \bar{c}_\text{II}\begin{pmatrix} x^{\text{in}}_{\text{II}} \\ p^{\text{in}}_{\text{II}} \end{pmatrix} + \bar{c}_\text{N,I}\begin{pmatrix} F^{\text{in}}_{x\text{I}} \\ F^{\text{in}}_{p\text{I}} \end{pmatrix} \qquad \text{(S.8)}\\
&+ \bar{c}_\text{N,II}\begin{pmatrix} F^{\text{in}}_{x\text{II}} \\ F^{\text{in}}_{p\text{II}} \end{pmatrix} + \bar{c}_\text{y}\begin{pmatrix} y^{\text{in}}_{\text{s},\bar{f}_\text{y}} \\ y^{\text{in}}_{\text{c},\bar{f}_\text{y}} \end{pmatrix} + \bar{c}_\text{q}\begin{pmatrix} q^{\text{in}}_{\text{c},\bar{f}_\text{q}} \\ -q^{\text{in}}_{\text{s},\bar{f}_\text{q}} \end{pmatrix}.
\end{aligned}$$

The modes appearing in this equation are defined as in Eq. (S.4) with

$$\begin{aligned}
\bar{f}_\text{N,I} &= \sqrt{2\gamma_\text{extra}}\Big(e^{-\gamma(T-t)} + \frac{Z\sqrt{2\gamma_\text{s}\gamma}g}{\sqrt{1-e^{-2\gamma T}}}\int_t^T dt' e^{-\gamma(2t'-t)}\\
&\quad [1-2\gamma_\text{s}(t'-t)]\Big),
\end{aligned}$$

$$\bar{f}_{\mathrm{N,II}} = \frac{Z\sqrt{\gamma_{\mathrm{s}}\gamma_{\mathrm{extra}}}}{\sqrt{\gamma}}\frac{g}{\sqrt{1-e^{-2\gamma T}}}\left(e^{-\gamma t}-e^{-2\gamma T}e^{\gamma t}\right),$$

$$\begin{aligned}\bar{f}_{\mathrm{y}} &= -\frac{\sqrt{2\gamma_{\mathrm{s}}}}{Z}e^{-\gamma(T-t)}+\frac{\gamma_{\mathrm{s}}}{\sqrt{\gamma}}\frac{g}{\sqrt{1-e^{-2\gamma T}}}\{\frac{2\gamma}{\gamma_{\mathrm{s}}}e^{-\gamma t}\\ &- [e^{-\gamma t}(2-\frac{\gamma_{\mathrm{s}}}{\gamma})-e^{-2\gamma T}e^{\gamma t}(2-\frac{\gamma_{\mathrm{s}}}{\gamma}-2\gamma_{\mathrm{s}}(T-t))]\},\end{aligned}$$

$$\begin{aligned}\bar{f}_{\mathrm{q}} &= \sqrt{2\gamma_{\mathrm{s}}}Z\{e^{-\gamma(T-t)}+\frac{Zg\sqrt{\gamma_{\mathrm{s}}}}{\sqrt{2\gamma}\sqrt{1-e^{-2\gamma T}}}[e^{-\gamma t}(2-\frac{\gamma_{\mathrm{s}}}{\gamma})\\ &- e^{-2\gamma T}e^{\gamma t}(2-\frac{\gamma_{\mathrm{s}}}{\gamma}-2\gamma_{\mathrm{s}}(T-t))]\}.\end{aligned}$$

The corresponding normalization factors read

$$\bar{N}_{\mathrm{N,I/II}} = \int_0^T dt\bar{f}_{\mathrm{N,I/II}}(t)^2, \quad \bar{N}_{\mathrm{y/q}} = \frac{1}{2}\int_0^T dt\bar{f}_{\mathrm{y/q}}(t)^2,$$

and the coefficients appearing in Eq. (S.8) are given by

$$\begin{aligned}\bar{c}_{\mathrm{I}} &= e^{-\gamma T}+\frac{gZ\sqrt{\gamma_{\mathrm{s}}}}{\sqrt{2\gamma}}(\sqrt{1-e^{-2\gamma T}}[1-\frac{\gamma_{\mathrm{s}}}{\gamma}]\\ &+ 2\gamma_{\mathrm{s}}T\frac{e^{-2\gamma T}}{\sqrt{1-e^{-2\gamma T}}}),\\ \bar{c}_{\mathrm{II}} &= \frac{gZ\sqrt{\gamma_{\mathrm{s}}}}{\sqrt{2\gamma}}\sqrt{1-e^{-2\gamma T}},\\ \bar{c}_{\mathrm{N,I}} &= \sqrt{\bar{N}_{\mathrm{N,I}}},\quad \bar{c}_{\mathrm{N,II}}=\sqrt{\bar{N}_{\mathrm{N,II}}},\quad \bar{c}_{\mathrm{y}}=\sqrt{\bar{N}_{\mathrm{y}}},\quad \bar{c}_{\mathrm{q}}=\sqrt{\bar{N}_{\mathrm{q}}}.\end{aligned}$$

All coefficients and mode functions in the input-output equation for the final atomic state Eq. (S.8) carry a bar in order to avoid confusion with the coefficients and mode functions appearing in the readout equation Eq. (S.1) in Sec. A.

2. *Teleportation fidelity*

The performance of the protocol is assessed using the average fidelity with respect to a Gaussian distribution of coherent input states as figure of merit. The fidelity $F=|\langle\Psi_{\mathrm{I}}^{\mathrm{tele}}|\Psi_{\mathrm{I}}^{\mathrm{opt}}\rangle|^2$ is given by the overlap of the final atomic state in ensemble I (Bob's state), $|\Psi_{\mathrm{I}}^{\mathrm{tele}}\rangle$, which is described by $x_{\mathrm{I}}^{\mathrm{tele}}$ and $p_{\mathrm{I}}^{\mathrm{tele}}$ and the optimal final state which is defined by the initial state in ensemble II (Charlie's state) $x_{\mathrm{II}}^{\mathrm{in}}$, $p_{\mathrm{II}}^{\mathrm{in}}$. For a given coherent input state with mean values $\langle x_{\mathrm{II}}\rangle$ and $\langle p_{\mathrm{II}}\rangle$ (and variances $\mathrm{var}(x_{\mathrm{II}})=\mathrm{var}(p_{\mathrm{II}})=1/2$), the single-shot fidelity is given by

$$F(\langle x_{\mathrm{II}}\rangle,\langle p_{\mathrm{II}}\rangle) = 2\,\frac{e^{\frac{-\left(|\langle x_{\mathrm{II}}\rangle|-|\langle x_{\mathrm{I}}^{\mathrm{tele}}\rangle|\right)^2}{1+2\mathrm{var}(x_{\mathrm{I}}^{\mathrm{tele}})}}\;e^{\frac{-\left(|\langle p_{\mathrm{II}}\rangle|-|\langle p_{\mathrm{I}}^{\mathrm{tele}}\rangle|\right)^2}{1+2\mathrm{var}(p_{\mathrm{I}}^{\mathrm{tele}})}}}{\sqrt{\left(1+2\mathrm{var}(x_{\mathrm{I}}^{\mathrm{tele}})\right)\left(1+2\mathrm{var}(p_{\mathrm{I}}^{\mathrm{tele}})\right)}},$$

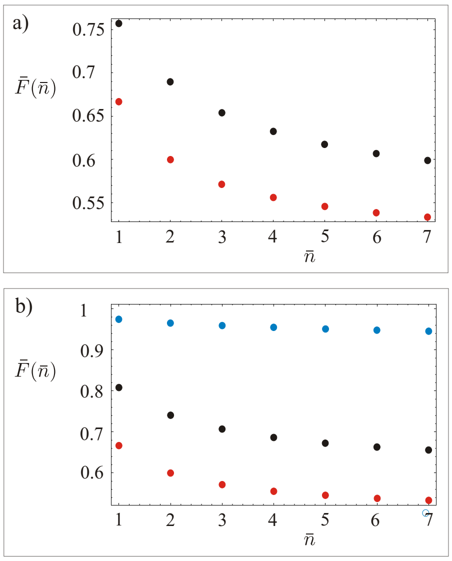

Supplementary figure S.1: Average teleportation fidelity $\bar{F}(\bar{n})$ for optimal gain g versus width of the distribution of input states $\bar{n}$. The lowest (red) line in both panels represents the classical benchmark. a) Teleportation fidelity for the measured experimental parameters (see methods). b) Maximum teleportation fidelity in the absence of losses. The curve in the middle (black) shows the attainable teleportation fidelity for the interaction used in the experiment ($Z=2.5$). The upmost curve (blue) depicts the QND-fidelity (for $Z\to\infty$, $\gamma_{\mathrm{s}}TZ^2=\mathrm{const}$) for exponentially shaped driving pulses (compare text, Sec. B 2).

such that the average fidelity $\bar{F}(\bar{n})$ with respect to a Gaussian distribution with width $\bar{n}$,

$$\begin{aligned}\bar{F}(\bar{n}) &= \frac{1}{2\pi\bar{n}}\int\!\!\int_{-\infty}^{\infty} d\langle x_{\mathrm{II}}\rangle d\langle p_{\mathrm{II}}\rangle F(\langle x_{\mathrm{II}}\rangle,\langle p_{\mathrm{II}}\rangle)e^{-\frac{\langle x_{\mathrm{II}}\rangle^2+\langle p_{\mathrm{II}}\rangle^2}{2\bar{n}}},\\ &= \frac{\sqrt{2}}{\sqrt{1+2\mathrm{var}\left(x_{\mathrm{I}}^{\mathrm{tele}}\right)+2\bar{n}\left(1-\left|\frac{\langle x_{\mathrm{I}}\rangle}{\langle x_{\mathrm{II}}\rangle}\right|\right)^2}}\\ &\quad\frac{\sqrt{2}}{\sqrt{1+2\mathrm{var}\left(p_{\mathrm{I}}^{\mathrm{tele}}\right)+2\bar{n}\left(1-\left|\frac{\langle p_{\mathrm{I}}\rangle}{\langle p_{\mathrm{II}}\rangle}\right|\right)^2}}.\end{aligned} \tag{S.9}$$

Both ensembles are initialized in a coherent spin state with $\langle x_{\mathrm{I}}\rangle=\langle x_{\mathrm{II}}\rangle=0$ and $\langle x_{\mathrm{I}}^2\rangle=\langle x_{\mathrm{II}}^2\rangle=1/2$. The photonic modes are also initially in the vacuum state, such that

$$\begin{aligned}|\langle x_{\mathrm{I}}\rangle/\langle x_{\mathrm{II}}\rangle| &= |\langle p_{\mathrm{I}}\rangle/\langle p_{\mathrm{II}}\rangle|=\bar{c}_{\mathrm{II}},\\ \mathrm{var}(x_{\mathrm{I}}^{\mathrm{tele}}) &= =\frac{1}{2}\left(\bar{c}_{\mathrm{I}}^2+\bar{c}_{\mathrm{II}}^2+m\bar{c}_{\mathrm{N,I}}^2+m\bar{c}_{\mathrm{N,II}}^2+\bar{c}_{\mathrm{y}}^2+\bar{c}_{\mathrm{q}}^2\right),\\ \mathrm{var}(p_{\mathrm{I}}^{\mathrm{tele}}) &= \mathrm{var}(x_{\mathrm{I}}^{\mathrm{tele}})\end{aligned}$$

Fig. S.1 shows the average teleportation fidelity $\bar{F}(n)$ in comparison to the classical limit $F_{\mathrm{clas}}=(1+\bar{n})\,/\,(1+2\bar{n})$, which cannot be surpassed by classical means [S9, S10, S11]. This figure also displays the average fidelity which can be achieved using a QND-interaction (i.e. for very large detuning, see Sec. A) if the classical driving pulses are modulated in time. These results have been obtained by considering different exponential functions $f_{\text{I}}(t) \propto e^{f_{\text{I}} t}$ and $f_{\text{II}}(t) \propto e^{f_{\text{II}} t}$ for the pulse shape of the classical field in the first and second interaction. The fidelity is optimized with respect to f_{I} and f_{II}. Fig. S.1b shows that fidelities close to one can be obtained in principle.

[S1] A. Silberfarb, I.H. Deutsch, Phys. Rev. A **68**, 13817 (2003).

[S2] L.B. Madsen, K. Mølmer, Phys. Rev. A, **70**, 052324 (2004).

[S3] K. Hammerer, E.S. Polzik, and J.I. Cirac, Phys. Rev. A **72**, 052313 (2005).

[S4] C.A. Muschik, H. Krauter, K. Jensen, J.M. Petersen, J.I. Cirac, and E.S. Polzik, J. Phys. B: At. Mol. Opt. Phys. **45**, 124021 (2012).

[S5] K. Hammerer, A. Sørensen, and E.S. Polzik, Rev. Mod. Phys. **82**, 1041 (2010).

[S6] C.A. Muschik, E.S. Polzik, and J.I. Cirac, Phys. Rev. A **83**, 052312 (2011).

[S7] D. V. Vasilyev, K. Hammerer, N. Korolev, A. S. Sorensen, J. Phys. B: At. Mol. Opt. Phys. **45**, 124007 (2012).

[S8] D. V. Vasilyev and Klemens Hammerer, personal communication.

[S9] A. Furusawa, J.L. Sørensen, S. L. Braunstein, C. A. Fuchs, H.J. Kimble and E.S. Polzik, Science **282**, 706 (1998).

[S10] S.L. Braunstein, H.J. Kimble and C.A. Fuchs, J. Mod. Opt. **47**,267 (2000).

[S11] K. Hammerer, M. M. Wolf, E. S. Polzik and J. I. Cirac, Phys. Rev. Lett. **94**, 150503 (2005).